Study of electromagnetic showers in water with the

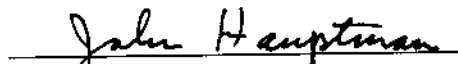Landau-Pomeranchuk-Migdal effect at very high energies

by

Panagiotis Dervenagas

A Thesis Submitted to the

Graduate Faculty in Partial Fulfillment of the

Requirements for the Degree of

MASTER OF SCIENCE

Department: Physics and Astronomy
Major: High Energy Physics

Approved:

John Hauptman
In Charge of Major Work

_____
For the Major Department

_____
For the Graduate College

Iowa State University
Ames, Iowa
1992

LIST OF FIGURES

CHAPTER 1. INTRODUCTION

The DUMAND[1] project, currently under construction in Hawaii, will be used to study high energy neutrino interactions. DUMAND may be operational as a detector with an area of 20000 m^2 and a volume of 2 10^6 m^3 of sea water in a few years. The detector will consist of strings of photomultiplier(PM) tubes located several thousand meters below the surface of the pacific.

Possible sources of neutrinos detectable in such PM tube arrays are atmospheric neutrinos, neutrinos from accelerators, and very high energy neutrinos generated by violent astrophysical processes. Proposed sources of neutrinos with energies up to 10^{16} eV are the, so called, Active Galactic Nuclei.

Of special interest is the case where a neutrino interacts with an electron to produce a W^- boson.

$$\bar{\nu}_e + e^- \rightarrow W^- \rightarrow \bar{\nu}_e + e^-$$

This is so because at the resonanse, where the center of mass energy is equal to the mass of the W^-, the cross section for the above reaction becomes very high. The resonant energy for this reaction is 6.4 10^{15} eV. So the electron produced from the decay of the W^- will have energy up to 6.4 10^{15} eV. This electron will generate an *electromagnetic cascade shower*, and the purpose of the present work is to study

---

[1] Deep Underwater Muon And Neutrino Detector

such *showers*.

At high energies the cross sections for *bremsstrahlung* and *pair production* should decrease in dense media (here water) due to the so called Landau-Pomeranchuk - Migdal effect (LPM effect). This is in contrast to the 'classical' Bethe- Heitler (BH) cross sections which are energy independent at high energies. Our calculations are based on the LPM cross sections.

In Chapter 2 we review *electromagnetic showers* and we introduce the LPM effect, and in Chapter 3 we describe the method we used to simulate the *electromagnetic showers*. The last two Chapters present the results and our conclusions.

Obviously, an *electromagnetic shower* can also be initiated by a photon.

The Bethe-Heitler theory

Bethe and Heitler in 1934 calculated the cross sections for *bremsstrahlung*. It turns out that the radiative processes of electrons take place at distances from the nucleus that are large compared with the nuclear radius. So, the screening effect of the atomic electrons is often important. Bethe and Heitler treated this effect using the Fermi-Thomas model of the atom. They found that the importance of screening in a radiation process, in which an electron of energy E_o emits a photon with fractional energy v, where $v = W/E_o$ and W is the energy of the photon, is determined by the quantity,

$$\gamma = 100 \frac{m_e c^2}{E_o} \frac{v}{1-v} Z^{-1/3} \tag{2.1}$$

where Z is the atomic number of the medium and m_e is the mass of the electron. The screening is more important for smaller γ. When γ is close to zero we have 'complete' screening. As E_o becomes larger γ decreases for given v. If E_o is large enough (say greater than 10^9 eV), screening can be considered as 'complete' for all photon energies. Since we are going to consider very high energies we give below only the formulas which correspond to the case of 'complete' screening ($\gamma \approx 0$).

Let us define here the concepts of *radiation length* and *critical energy*, which are very useful in shower theory.

The *radiation length* is that thickness of a medium which reduces the mean energy of a beam of electrons by a factor of e. It is given, approximately, by [7]

$$X_o = \frac{716.4A}{Z(Z+1)ln(287\sqrt{Z})} \tag{2.2}$$

Here Z and A are the atomic number and mass number of the atoms of the medium. In the above formula X_o is given in g/cm^2. To express it in cm we just divide by the density.

The *radiation length* of a mixture or compound is approximated by

$$\frac{1}{X_o} = \sum_i \frac{f_i}{X_i} \tag{2.3}$$

where f_i and X_i are the fractional weight and the *radiation length* of the i_{th} element.

The *critical energy* E_c is defined as the energy where the average energy loss of an electron due to radiation is equal to the average energy loss due to *collision processes*. Above E_c radiation losses dominate, while below E_c ionization is more important. E_c is given approximately by

$$E_c = \frac{800\ MeV}{Z + 1.2} \tag{2.4}$$

After these definitions we are ready to consider the Bethe-Heitler(BH) result for *bremsstrahlung* in the case of 'complete' screening.

Let $\Phi_r^{BH}(E_o, v)dv$ denote the probability per radiation length that an electron of energy E_o will emit a photon of fractional energy in the interval $v + dv$ where $v = W/E_o$ and W is the energy of the photon. Then $\Phi_r^{BH}(E_o, v)dv$ is given by the expression, [1]

$$\Phi_r^{BH}(E_o, v)dv = \frac{1}{v}\left\{1 + (1 - v)^2 - (\frac{2}{3} - 2b)(1 - v)\right\}dv \tag{2.5}$$

where b is given by

$$b = \frac{1}{18ln(191Z^{-1/3})} \tag{2.6}$$

Of course the same formula is valid for positrons.

The photon is emited in some angle with respect to the electron initial direction. The root mean square angle of emission of photons can be expressed by

$$\langle \Theta^2 \rangle_{av}^{1/2} = q(E_o, W, Z) \frac{m_e c^2}{E_o} ln \frac{E_o}{m_e c^2} \qquad (2.7)$$

where $q(E_o, W, Z)$ is a function which is always of the order of magnitude of one.

Bethe and Heitler calculated in the same paper the cross setion for *pair production*. The phenomena of *bremsstrahlung* and *pair production* are closely related, so the formulas that describe them are very similar.

Again, the screening is important. For the case of a photon of energy W_o which produces an electron-positron pair, with the electron carrying fractional energy u, where $u = E/W_o$ and E is the energy of the electron, the importance of screening is determined by the quantity,

$$\gamma = 100 \frac{m_e c^2}{W_o} \frac{1}{u(1-u)} Z^{-1/3} \qquad (2.8)$$

The screening is more important the smaller the γ. When γ is close to zero we have 'complete' screening. As before, screening can be considered as 'complete' if the energy of the photon is greater than 10^9 eV. We only consider this case here.

Let $\Phi_p^{BH}(W_o, u)du$ denote the probability per radiation length that a photon of energy W_o will produce an electron-positron pair with the electron carrying fractional energy in the interval $u + du$ where $u = E/W_o$ and E is the energy of the electron. Then $\Phi_p^{BH}(W_o, u)du$ is given by the expression,

$$\Phi_p^{BH}(W_o, u)du = \left\{ u^2 + (1-u)^2 + (\frac{2}{3} - 2b)u(1-u) \right\} du \qquad (2.9)$$

where b is the same as above.

$$\bar{s} = 1370 \left\{ \frac{W_o X_o}{E(W_o - E)} \right\}^{1/2} \tag{2.19}$$

$$\xi(s) = 1 + \left\{ \frac{\ln s}{\ln s_o} \right\} \quad , s \in [s_o, 1] \tag{2.20}$$

$$= 1 \quad , s > 1$$

$$= 2 \quad , s < s_o$$

where,

$$s_o^{1/2} = \frac{Z^{1/3}}{190} \tag{2.21}$$

Also,

$$G(s) = 48s^2 \left\{ \frac{\pi}{4} - \frac{1}{2} \int_0^\infty \frac{e^{-st} \sin(st)}{\sinh(t/2)} \, dt \right\} \tag{2.22}$$

and

$$\phi(s) = 12s^2 \int_0^\infty \coth(x/2) e^{-sx} \sin(sx) \, dx - 6\pi s^2 \tag{2.23}$$

Numerical values for G(s) and $\phi(s)$ are given in Table 2.1. In the limit that s approaches zero we have,

$$\lim_{s \to 0} G(s) = 12\pi s^2 \tag{2.24}$$

$$\lim_{s \to 0} \phi(s) = 6s \tag{2.25}$$

X_o is the radiation length of the medium expressed in centimeters. Note that equations (2.18) and (2.19) are in a system of units with $\hbar = c = m_e = 1$, so to use these two equations we need to divide all energies by the electron mass $m_e = 0.5 \ 10^6$

the final results are consistent with other calculations, and this justifies our choice.

Then a random number generator is used to give a random number in the interval (0,1). If this random number is less than 1/3, we have *bremsstrahlung* in this step (at the midlle of the step). Otherwise, we take further steps (with new random number each time), until we have the radiation process.

Since the random number generator is very important for our calculation, we give in Figure 3.1 a frequency distribution for one million random numbers given by the generator used. As we can see the distribution is very close to the ideal.

Now, we have to decide the energy of the radiated photon. This is done by taking a new random number r and finding the photon energy $W = E_o v$, by solving numerically the equation,

$$r \int_{10^{-5}}^{1-h} \Phi_r^{LPM}(E_O, v) \, dv = \int_{10^{-5}}^{v} \Phi_r^{LPM}(E_O, v) \, dv \qquad (3.3)$$

for v.

Pair production is treated in a very similar way. The total probability per radiation length is given by,

$$P_p^{LPM}(W_O) = \int_0^{1-g} \Phi_p^{LPM}(W_O, u) du \qquad (3.4)$$

where

$$g = \frac{2m_e c^2}{W_O} \qquad (3.5)$$

for the rest energy of the pair. Here we take the lower limit as zero, since there is no divergence problem. The same random number techniques are used to determine the point where the process takes place and the distribution of the energy in the electron-positron pair.

CHAPTER 4.   RESULTS

Following the procedure described in the previous chapter we obtain the distribution of the energy deposited in the water. This was done for four different *showers*. Since we are using random number techniques in the calculations, noticable variations in the final result are produced. Then we average the four *showers* to obtain an 'average' *shower*.

The longitudinal profile

The *showers* are very confined in the direction of the primary electron (see next section). That is, most of the particles travel along the z-direction, and most of the energy is deposited very close to the z-axis.

Therefore, a quantity of great interest is the energy deposited per unit length as a function of the distance travelled along the z-axis. In Figures 4.1, 4.3, 4.5 and 4.7 we give this result for the four different *showers*. The same results are presented in Figures 4.2, 4.4, 4.6 and 4.8 in logarithmic scale. The results for the 'average' *shower* are given in Figures 4.9 and 4.10.

We see that the energy deposit rises almost exponentially, reaches a maximum at about 20 radiation lengths, and drops again exponentially (slower this time). This is the typical profile for *electromagnetic showers* [7].
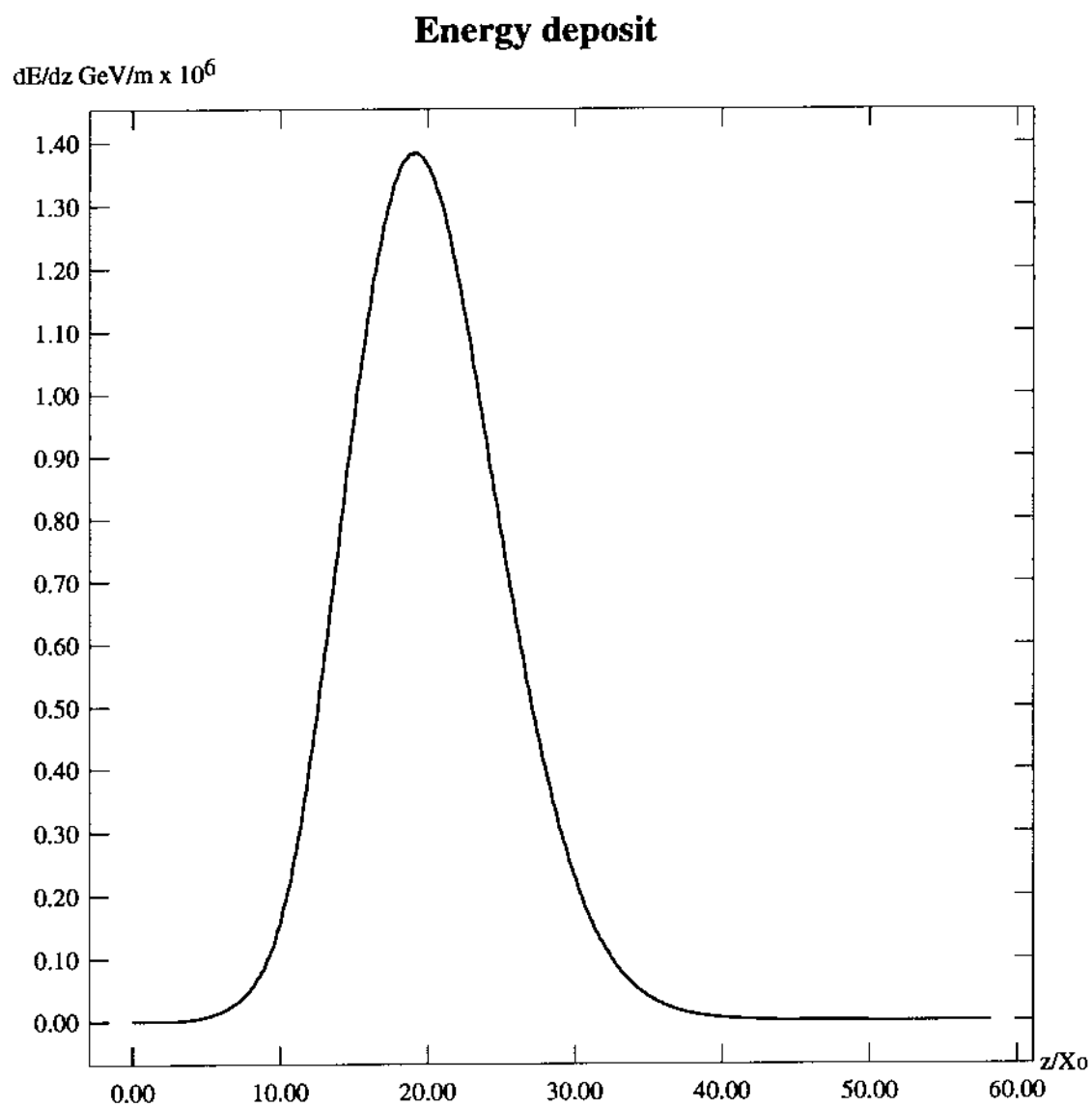
Energy deposit

dE/dz GeV/m x 10^6

Figure 4.1:   Energy deposit vs distance in the direction of the primary electron, for the first shower
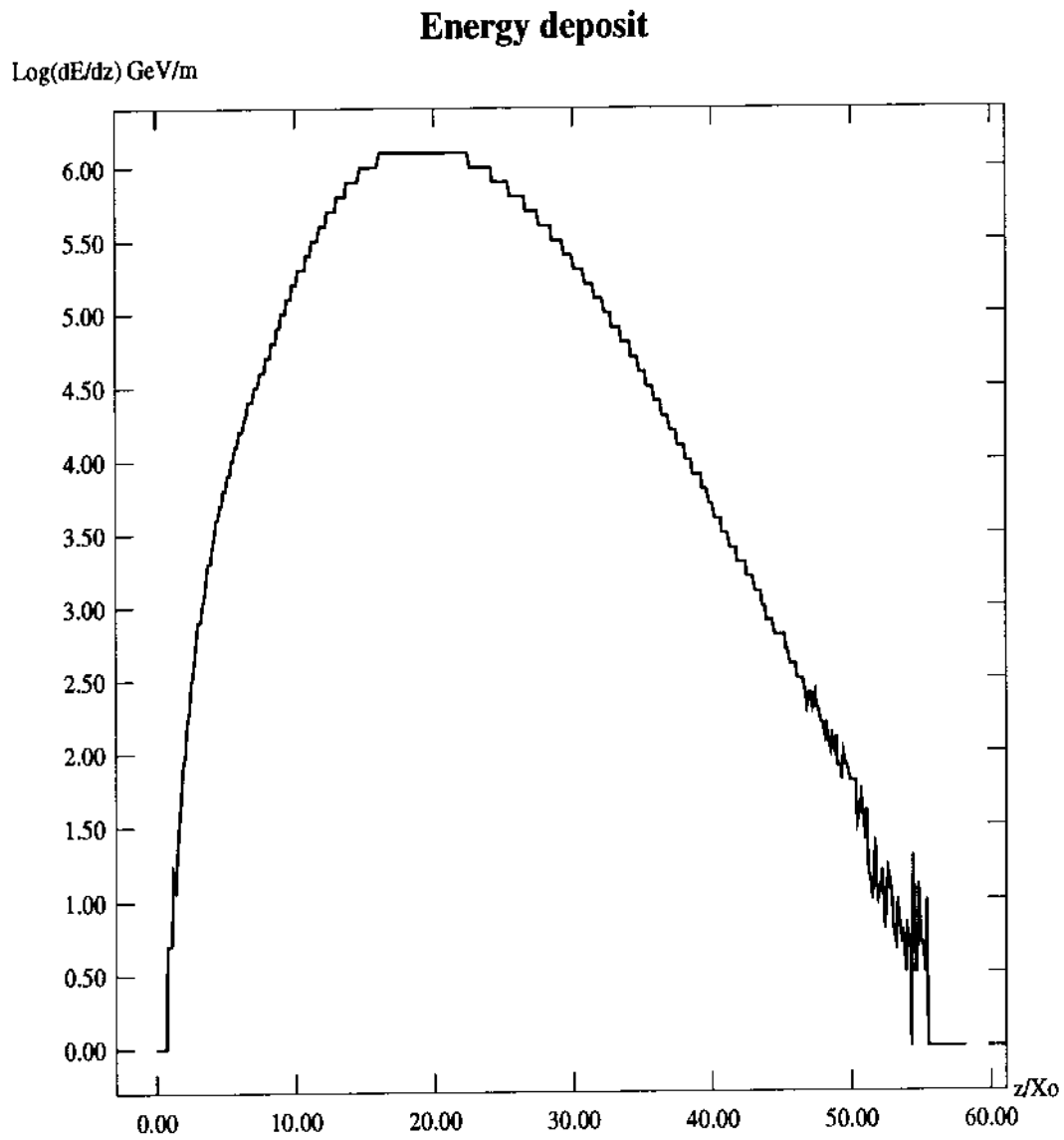
Energy deposit

Log(dE/dz) GeV/m

Figure 4.2: Energy deposit vs distance in the direction of the primary electron, for the first shower
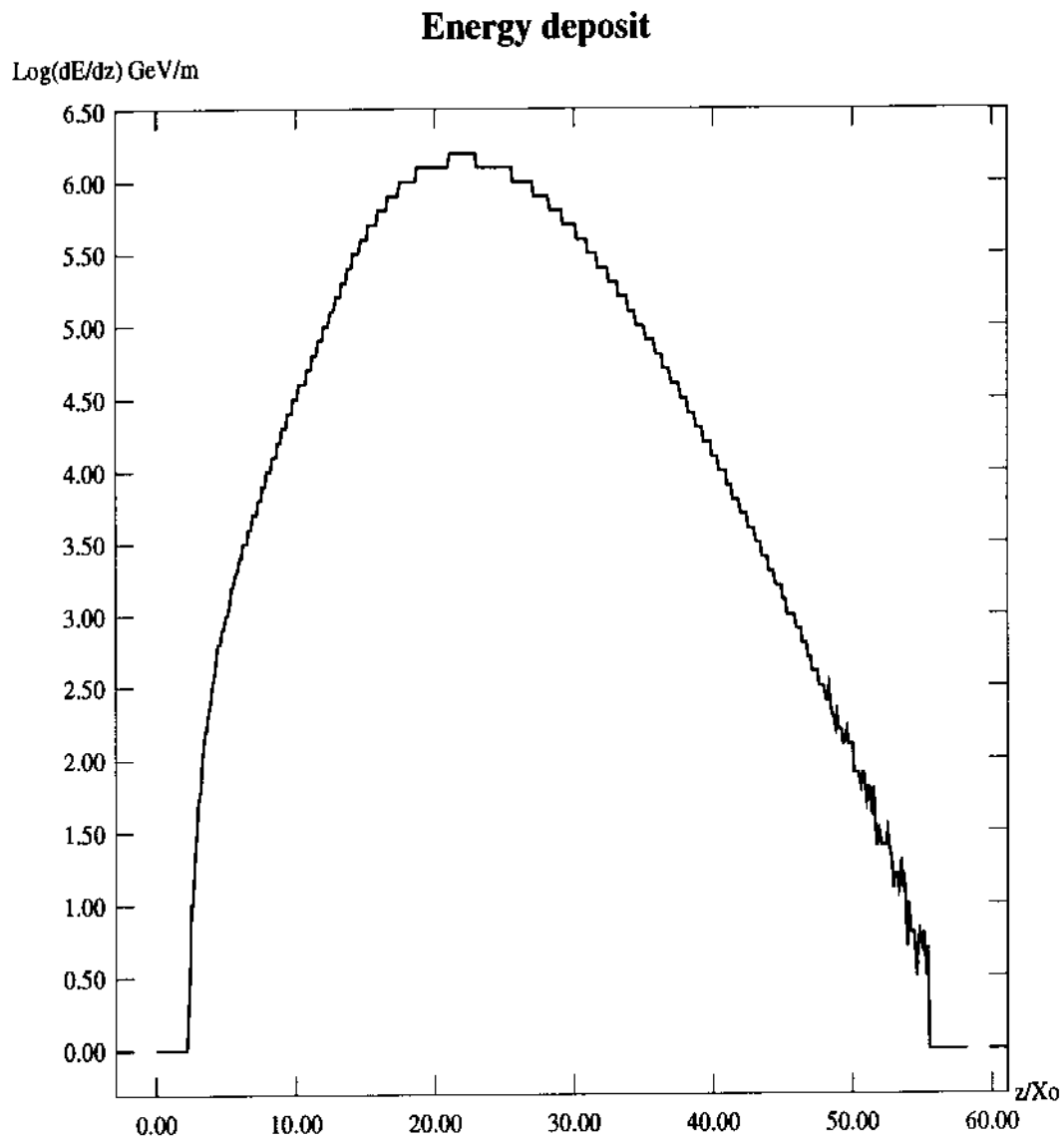
Energy deposit

dE/dz GeV/m x 10^6
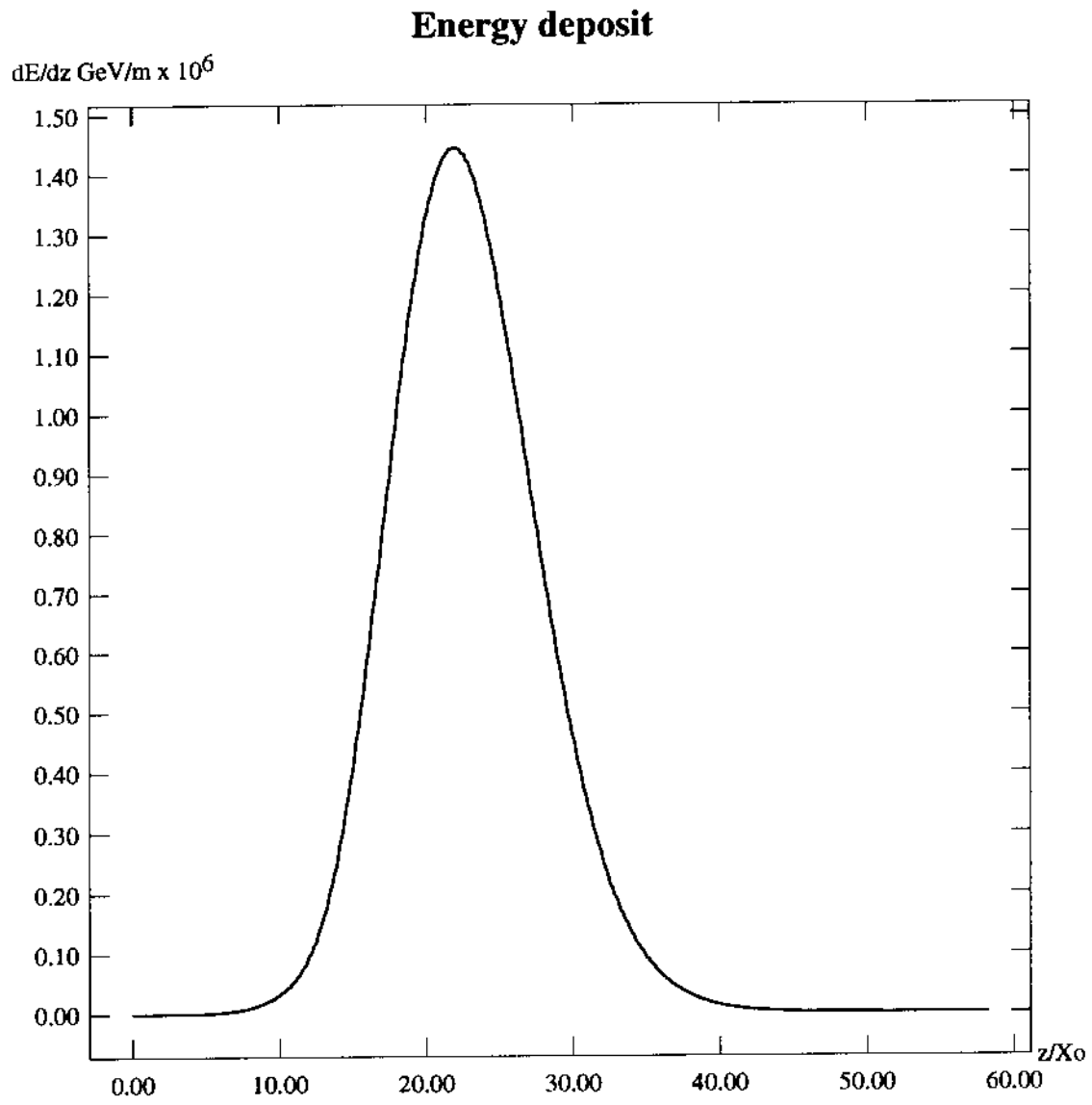
Figure 4.3: Energy deposit vs distance in the direction of the primary electron, for the second shower

Energy deposit

Log(dE/dz) GeV/m

Figure 4.4: Energy deposit vs distance in the direction of the primary electron, for the second shower
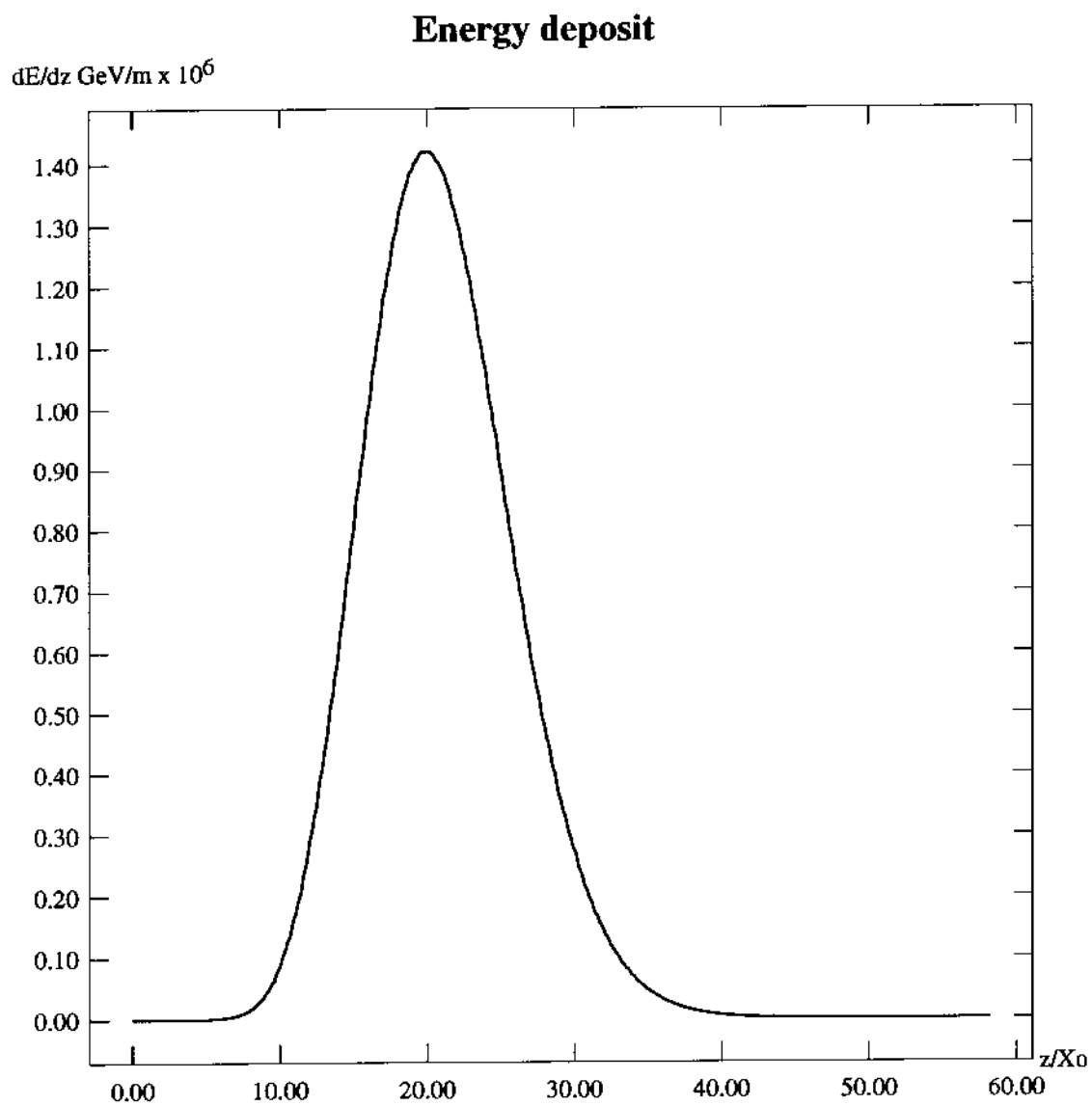
Energy deposit

dE/dz GeV/m x 10^6

Figure 4.5:   Energy deposit vs distance in the direction of the primary electron, for the third shower
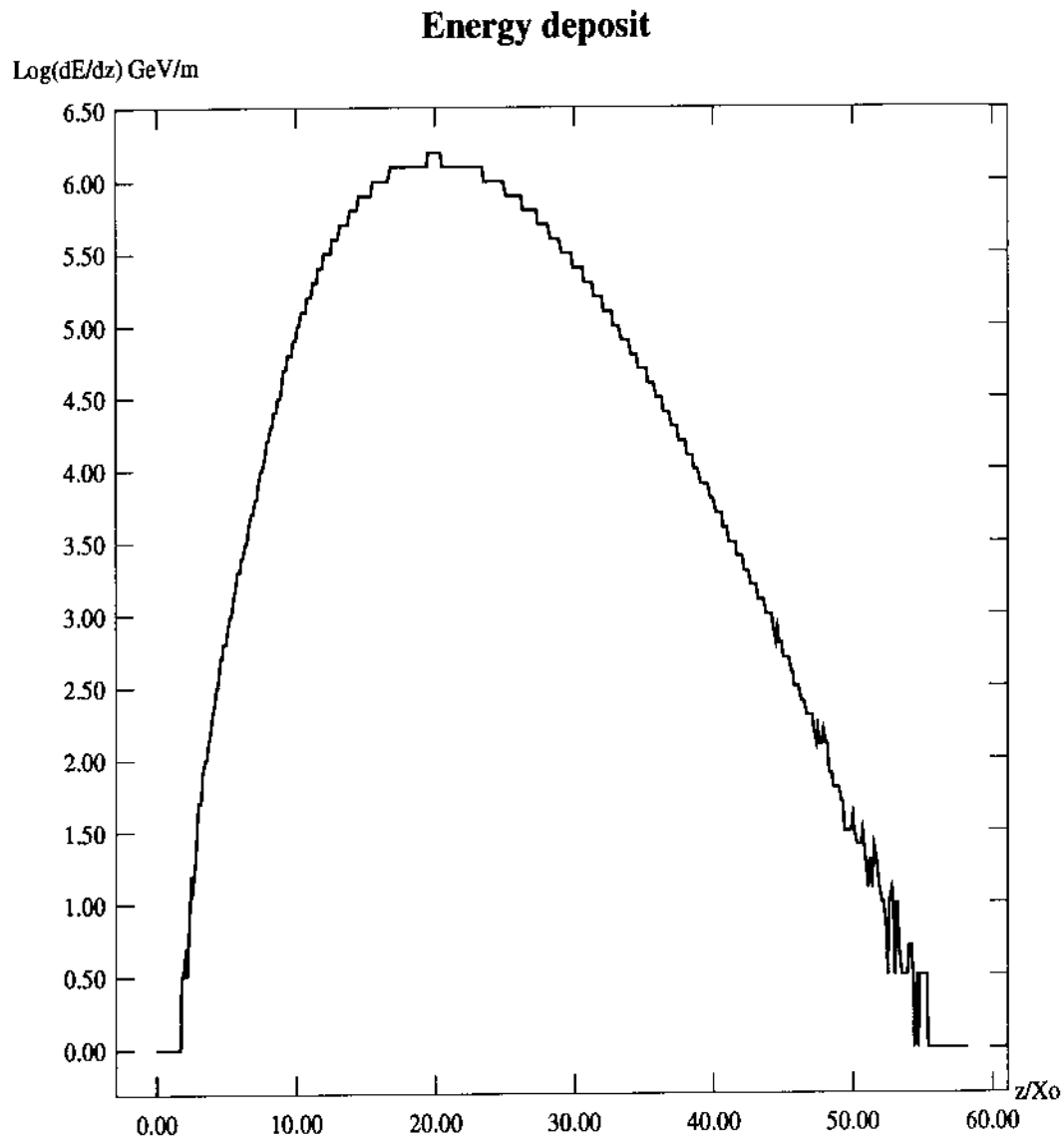
Energy deposit

Log(dE/dz) GeV/m

Figure 4.6: Energy deposit vs distance in the direction of the primary electron, for the third shower
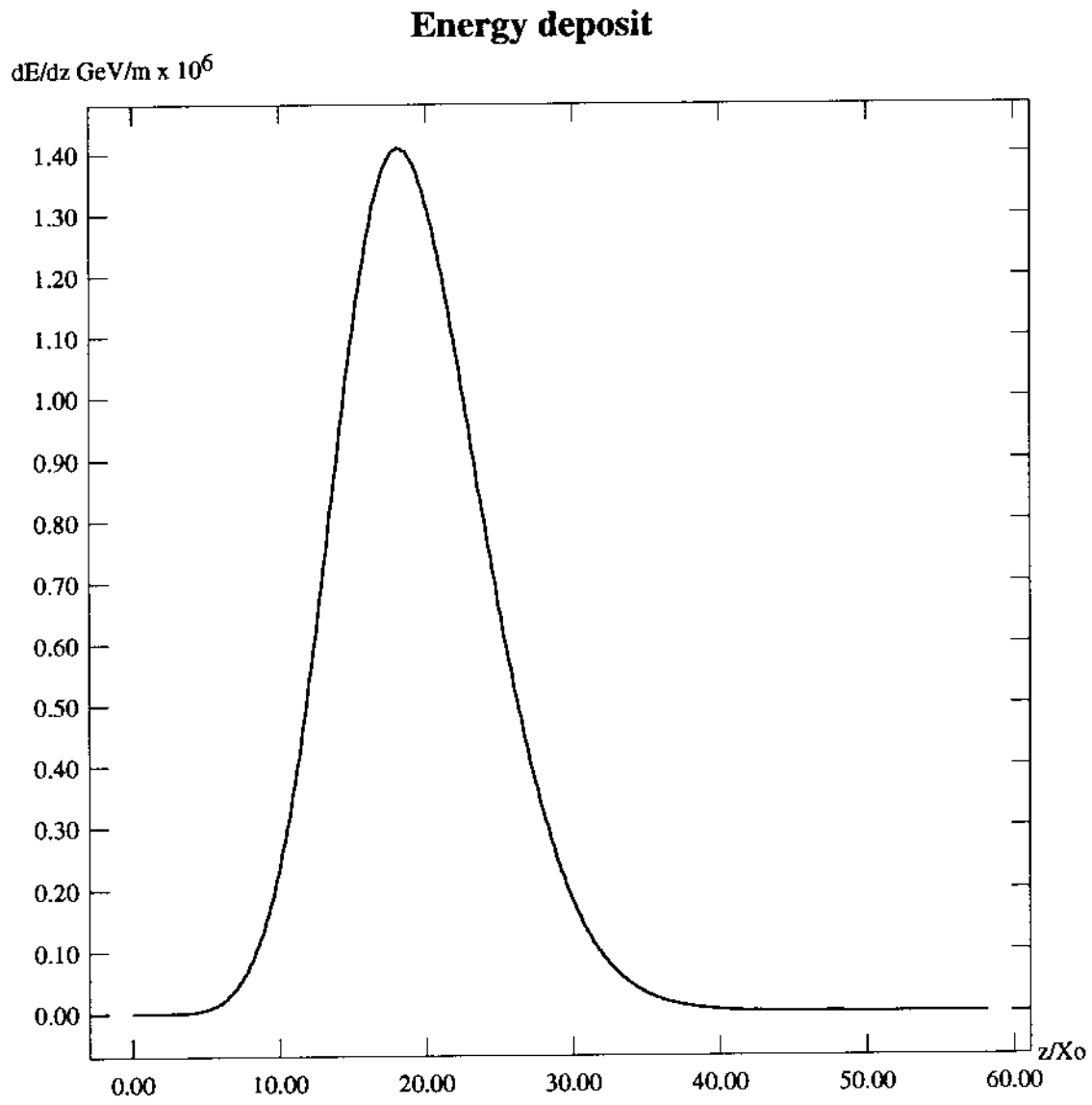
Energy deposit

dE/dz GeV/m x 10^6

Figure 4.7: Energy deposit vs distance in the direction of the primary electron, for the fourth shower
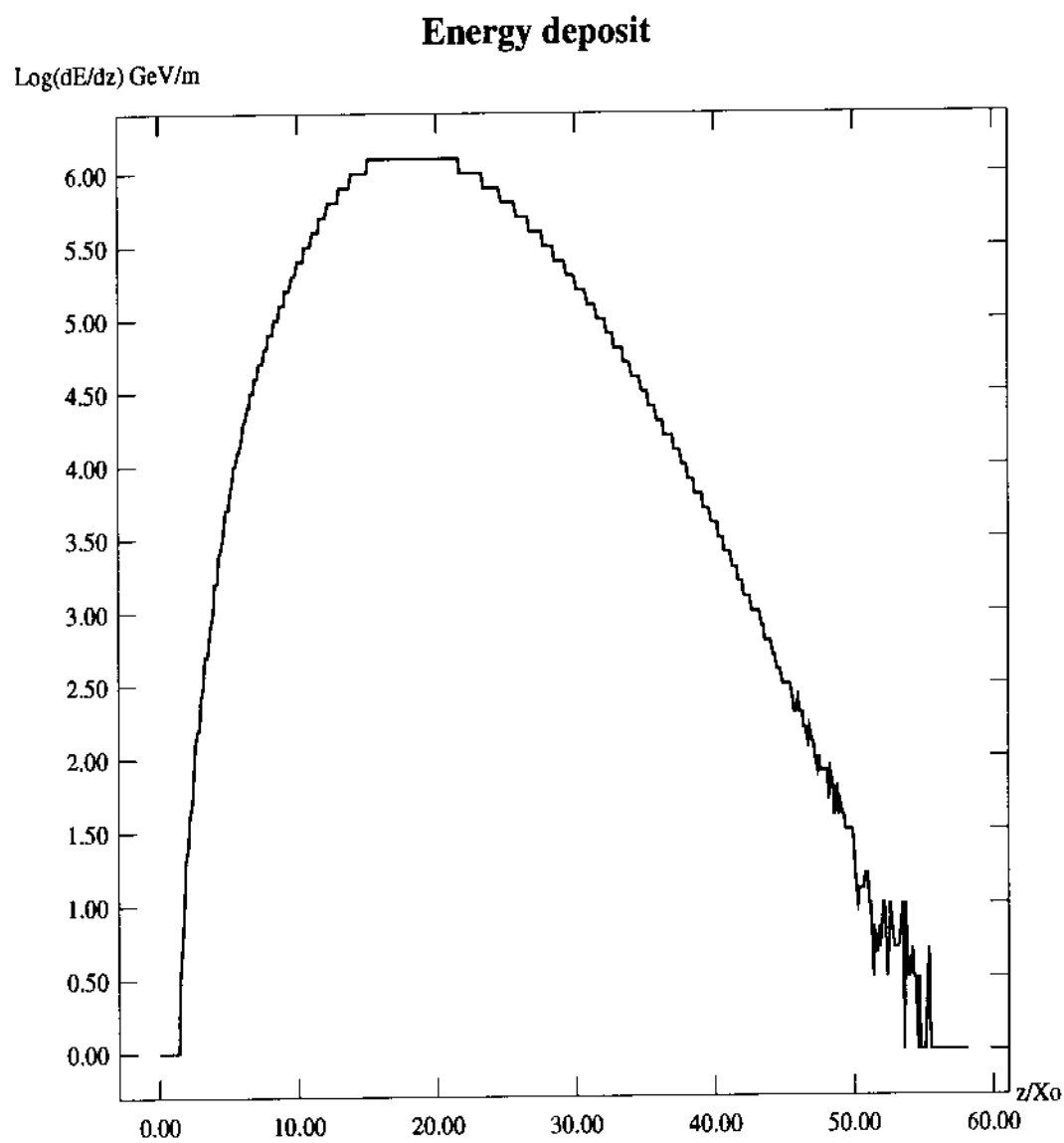
Energy deposit

Log(dE/dz) GeV/m

Figure 4.8:   Energy deposit vs distance in the direction of the primary electron, for the fourth shower

Energy deposit

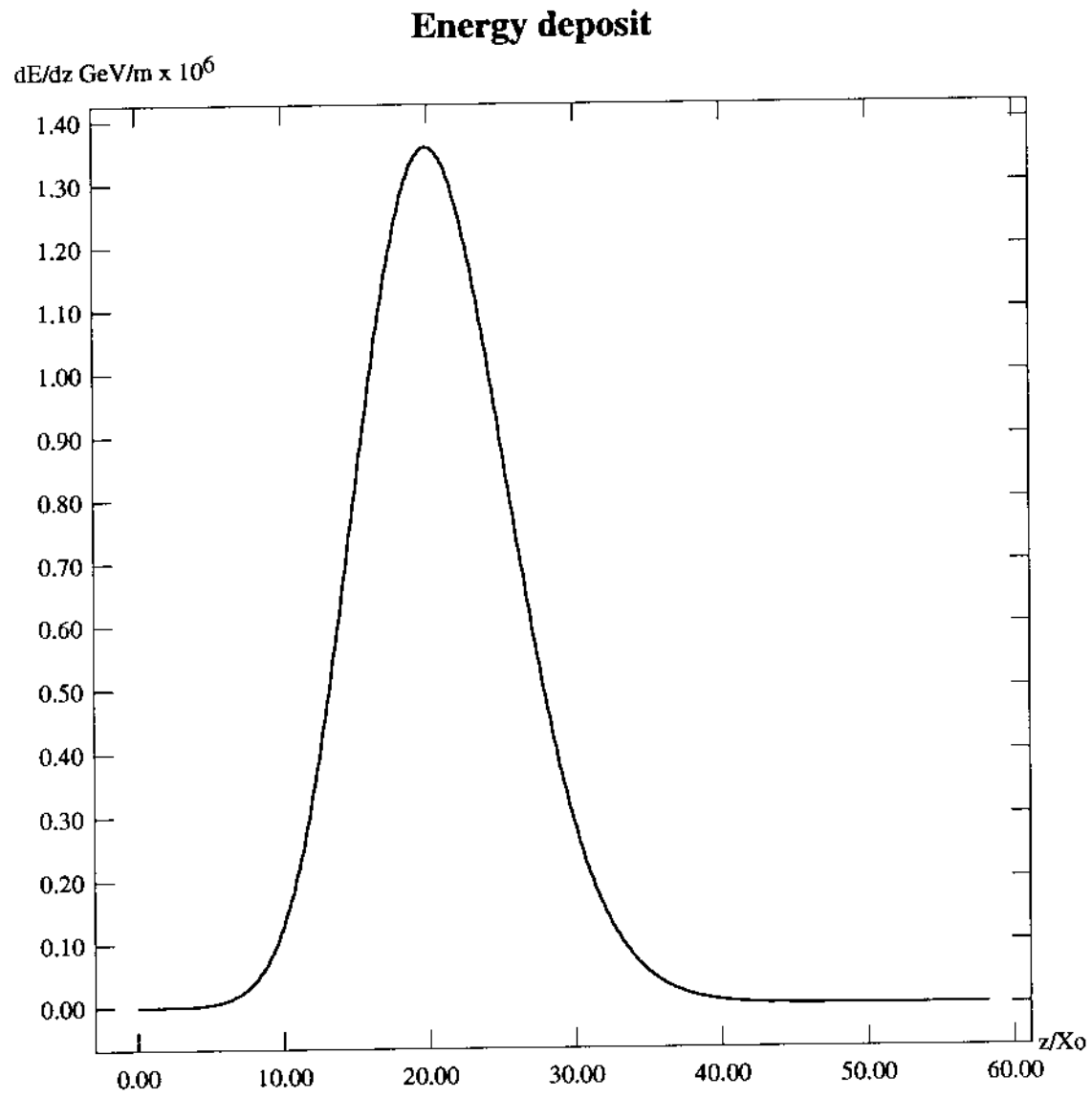dE/dz GeV/m x 10^6

z/X$_0$

Figure 4.9:   Energy deposit distance in the direction of the primary electron, for the 'average' shower

The transverse profile

Of course, the *showers* have some spreading in the xy plane (transverse plane). In Figures 4.11 and 4.12 we give the energy deposited per unit length, as a function of distance in the x-direction. It must be obvious that for certain x we integrate over all y and z. The same quantity for the y-direction is given in Figures 4.13 and 4.14. The above refer to the 'average' shower.

We observe that the *showers* develop very close to the z-axis. This is because for high energies the emitted particles travel almost in the same direction as the primary particle, as can be seen from formulas (2.7) and (2.10). As the energy decreases particles are emitted at larger angles. But these are low energy particles which lose all their energy before going too far. So the *showers* do not spread too much in the transverse direction. We also see that the distributions are almost the same along the x and y directions, as they should be because of symmetry.

Also, the *showers* are very narrow during the first stages of development and they spread out more in the final stages. We can see this by giving the same functions as above, but this time keeping z constant. That is for certain x we only integrate the y coordinate. This is done in Figures 4.15 to 4.19 where we give the energy deposited per unit length in the x-direction, for five different distances along the z-axis. As we can see, the *shower* is very narrow for small z where all the particles are emitted in very small angles, and it spreads out more as the energy of the particles decreases.
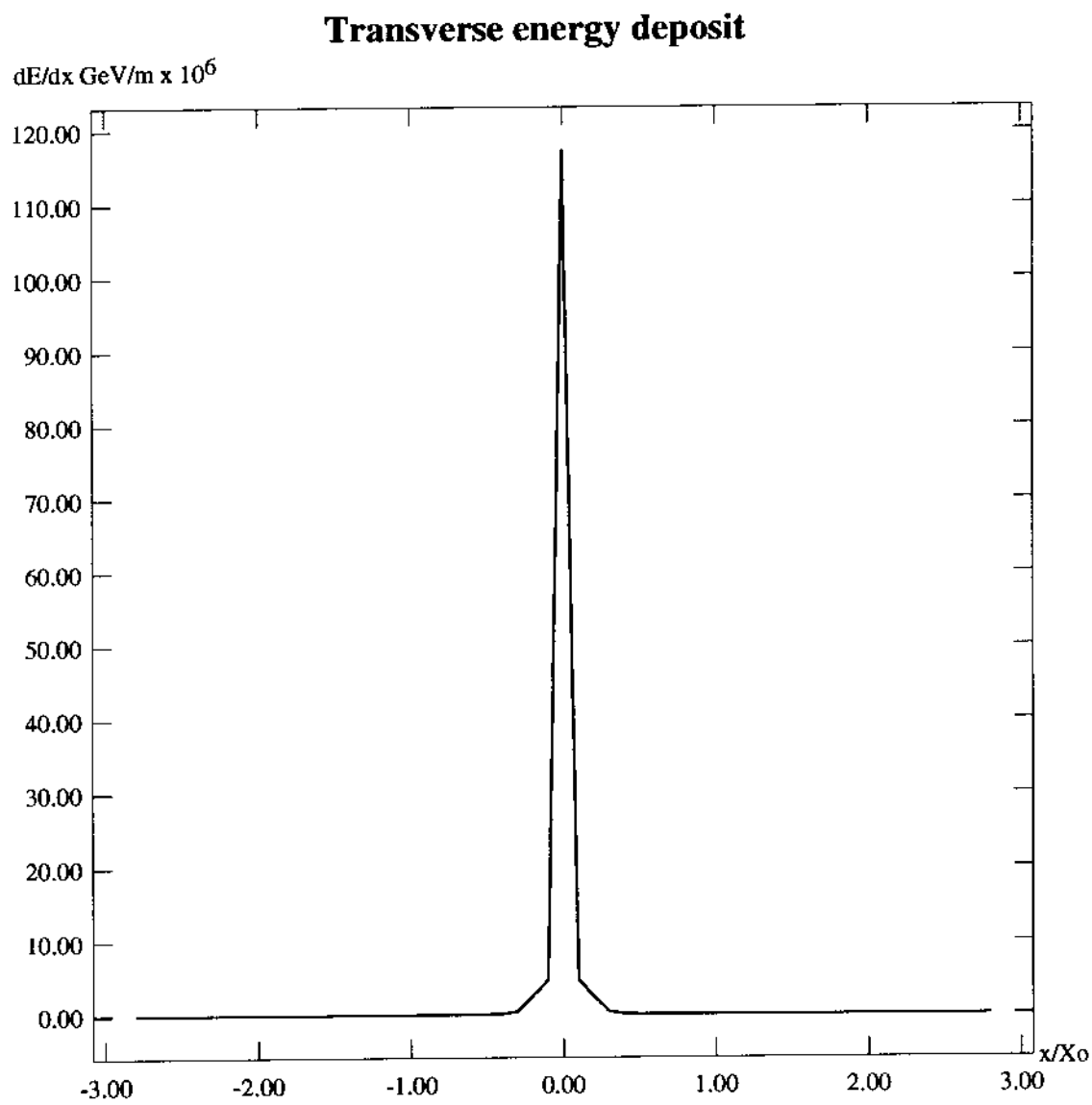
Transverse energy deposit

dE/dx GeV/m x 10^6

x/Xo

Figure 4.11:   Energy deposit vs distance in the x-direction for the 'average' shower

Transverse energy deposit

Log(dE/dx) GeV/m
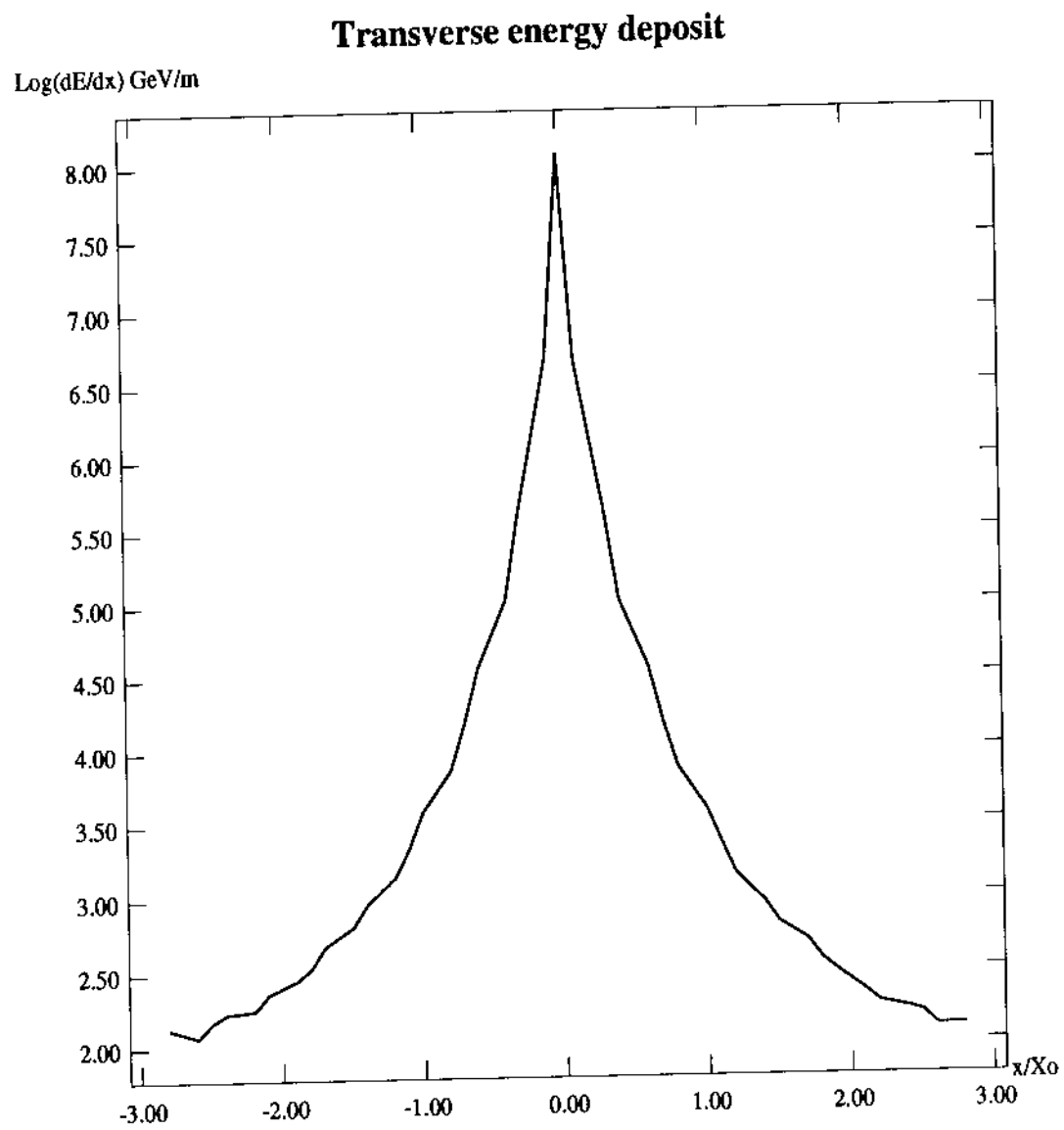
Figure 4.12: Energy deposit vs distance in the x-direction for the 'average' shower

Transverse energy deposit
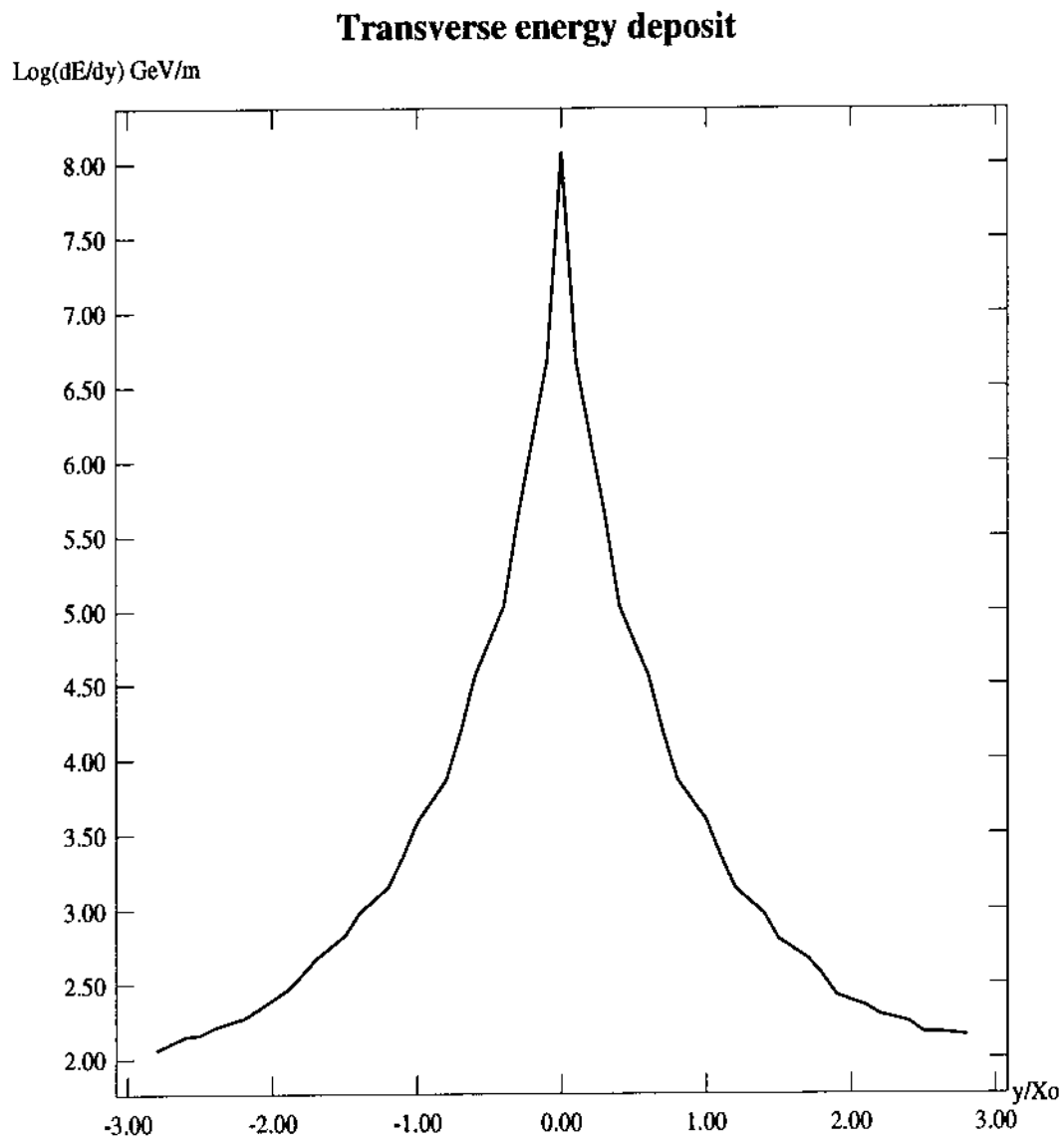
Figure 4.14:   Energy deposit vs distance in the y-direction for the 'average' shower

Transverse energy deposit for constant z
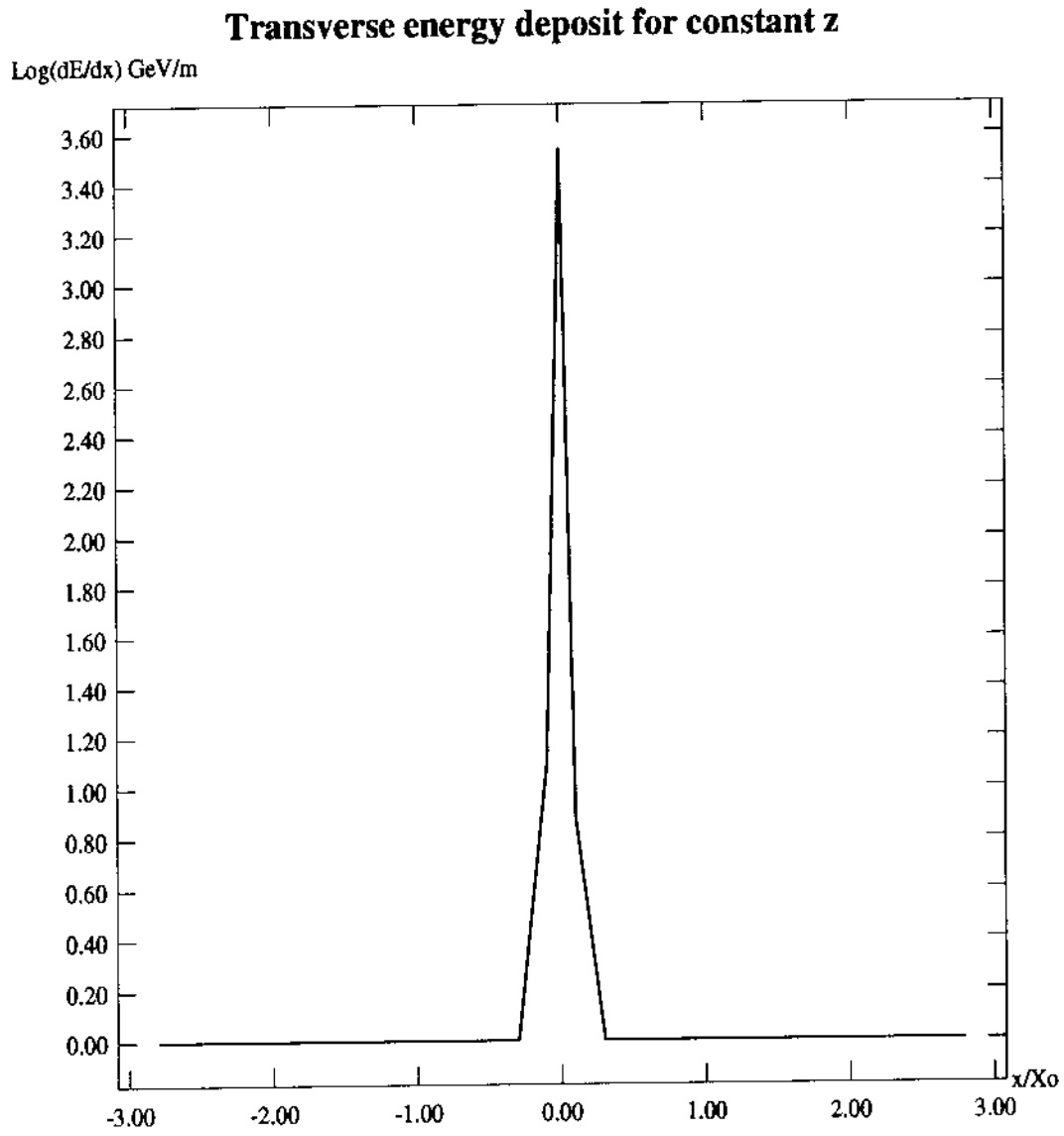
Figure 4.15:   Energy deposit in the x-direction at z=5 radiation lengths

Transverse energy deposit for constant z

Log(dE/dx) GeV/m
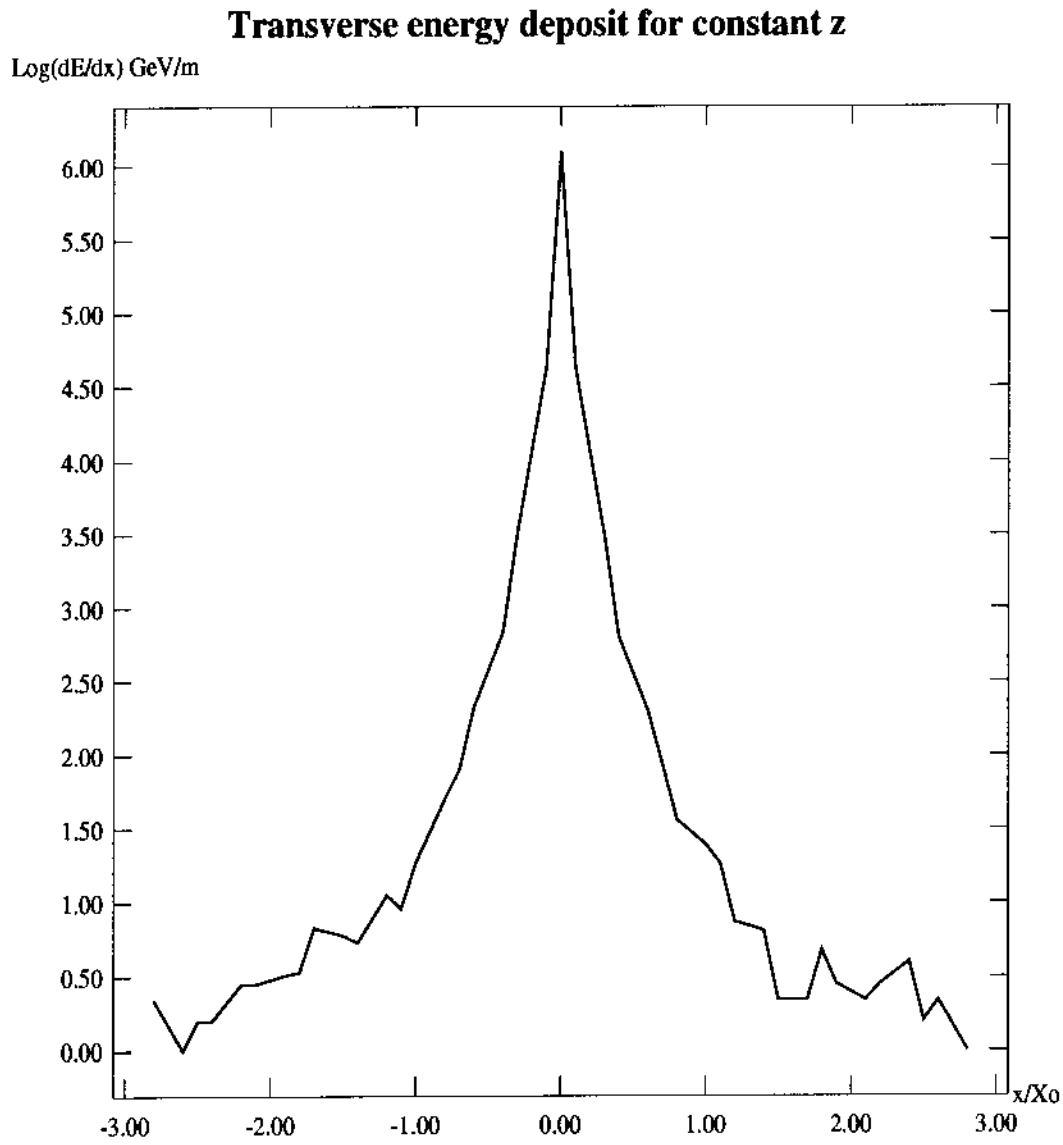
Figure 4.17:   Energy deposit in the x-direction at z=20 radiation lengths

Transverse energy deposit for constant z

Log(dE/dx) GeV/m
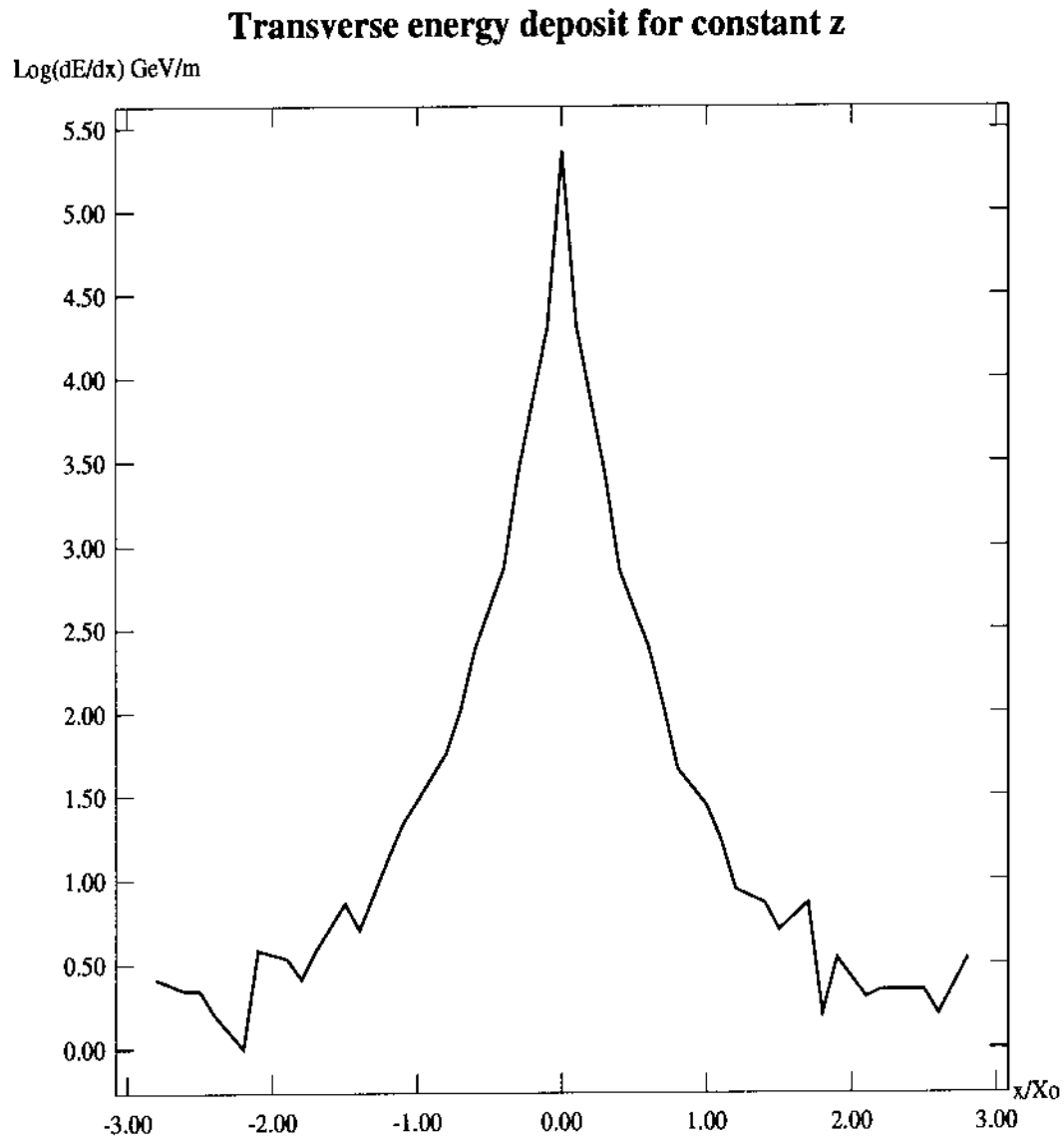
Figure 4.18: Energy deposit in the x-direction at z=30 radiation lengths

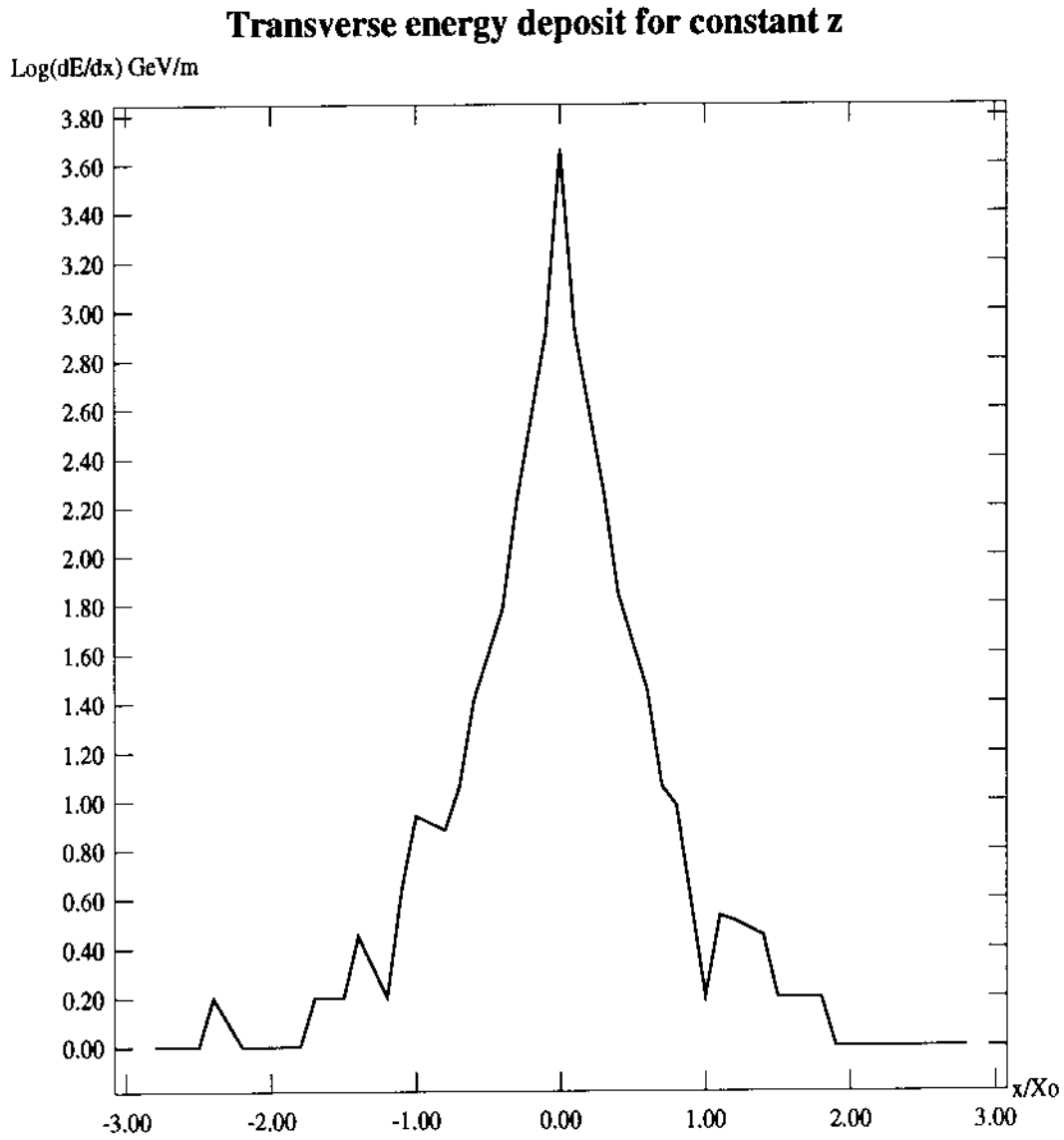**Transverse energy deposit for constant z**

Log(dE/dx) GeV/m

Figure 4.19: Energy deposit in the x-direction at z=40 radiation lengths

Comparison of the results with other calculations

Misaki [10] has also studied *electromagnetic showers* in water with the LPM effect, using an entirely different approach. He focuses mostly on the transition curves of electron number. In other words he calculates the number of electrons per unit length, as a function of the distance travelled in the direction of the primary particle. These curves are very similar to the ones we calculated for the energy deposited along the z-axis, that is, the shape of the curves is approximately the same and the maxima almost coincide [7].

In Table 4.1 we give Misaki's results for the depth of shower maximum T_{max} for various initial energies. We also give his results for the full width half maximum, FWHM, of the electron transition curves. The threshold energy for these values is 10^9 eV (only electrons with energy higher than the threshold are counted). The depth and the FWHM values are given in units of radiation length both for LPM and BH *showers*.

According to Table 4.1, the maximum depth for a *shower* with initial energy 6.4 10^{15} eV will be about 18 radiation lengths without the LPM effect and about 20 radiation lengths with the effect. Of course, this is for the electron transition curves, but as we said this maximum almost coincides with the one of the energy distribution curves. Also the FWHM for an LPM *shower* of the same energy is about 14 radiation lengths according to Table 4.1.

From Figures 4.9 and 4.10 we see that the maximum energy deposit for our showers occurs at about 20 radiation lengths, and the FWHM for our 'average' *shower* is about 13.2 radiation lengths. So our results are consistent with those obtained by Misaki.

Table 4.1:   Depth of shower maximum according to Misaki's calculations

E_o/eV	10^{15}	10^{16}	10^{17}	10^{18}	10^{19}	10^{20}	10^{21}
T_{max}^{LPM}	18	24	38	78	200	569	1696
T_{max}^{BH}	17	19	22	24	26	29	31
$FWHM^{LPM}$	13	16	28	75	223	676	2049
$FWHM^{BH}$	12	13	14	15	15	16	17

Table 4.1 also shows that the LPM effect is important for the energies we are considering, and if we go to even higher energies the difference with BH *showers* is really impressive. For instance at 10^{21} eV the maximum of a BH *shower* is at 31 radiation lengths, while for a LPM *shower* it is at 1696 radiation lengths !

BIBLIOGRAPHY

[1] Rossi, B. *High-Energy Particles*. New York: Prentice-Hall, Incorporated, 1952.

[2] Landau, L.D. and Pomeranchuk, I.J. *Doklady Akad. Nauk* SSSR 92, 535 (1953).

[3] Landau, L.D. and Pomeranchuk, I.J. *Doklady Akad. Nauk* SSSR 92, 735 (1953).

[4] Migdal, A.B. *Phys. Rev.* 103, 1811 (1956).

[5] Stanev, T. et al. *Phys. Rev. D* 25, 1291 (1982).

[6] Kasahara, K. *Phys. Rev. D* 31, 2737 (1985).

[7] 'Review of Particle Properties' *Phys. Rev. D* 45 (1992).

[8] Bethe, H.A. and Heitler, W. *Proc. Roy. Soc.* A146, 83 (1934).

[9] *GEANT3 User's guide*, CERN DD/EE/84-1 (1987).

[10] Misaki, A. *Fortschr. Phys.* 38, 6 ,413 (1990).

[11] Klein, S. et al. SLAC-PUB-5969, (1992).